

Data-Driven Stochastic Optimal Control in Reproducing Kernel Hilbert Spaces [★]

Nicolas Hoischen^a, Petar Bevanda^a, Stefan Sosnowski^a, Sandra Hirche^a, Boris Houska^b

^a*Chair of Information-oriented Control, TU Munich, Germany*

^b*School of Information Science and Technology, ShanghaiTech University, China*

Abstract

This paper proposes a fully data-driven approach for optimal control of nonlinear control-affine systems represented by a stochastic diffusion. The focus is on the scenario where both the nonlinear dynamics and stage cost functions are unknown, while only a control penalty function and constraints are provided. To this end, we embed state probability densities into a reproducing kernel Hilbert space (RKHS) to leverage recent advances in operator regression, thereby identifying Markov transition operators associated with controlled diffusion processes. This operator learning approach integrates naturally with convex operator-theoretic Hamilton–Jacobi–Bellman recursions that scale linearly with state dimensionality, effectively solving a wide range of nonlinear optimal control problems. Numerical results demonstrate its ability to address diverse nonlinear control tasks, including the depth regulation of an autonomous underwater vehicle.

Keywords: stochastic optimal control problems, learning methods for optimal control, operator theory, data-driven control theory, kernel methods

1. Introduction

Data-driven control methods offer a compelling alternative when deriving accurate first-principle models becomes prohibitively complex. Classical approaches retain structural knowledge of the system dynamics while using data to estimate unknown parameters through system identification and adaptive control techniques (Astrom and Wittenmark, 1994). As system complexity grows, methods relying less on prior knowledge have emerged: Gaussian processes learn unknown dynamics with quantified uncertainty (Hewing et al., 2019), data-enabled predictive control synthesizes controllers directly from input-output data (Coulson et al., 2019), and reinforcement learning methods such as (Schulman et al., 2017) learn optimal policies through direct environmental interaction, surpassing traditional model-based optimal control—for example, in agile drone racing (Song et al., 2023). This spectrum, from

[★]This work was supported by the DAAD program Konrad Zuse Schools of Excellence in Artificial Intelligence, sponsored by the Federal Ministry of Education and Research, and by the European Union’s Horizon Europe innovation action program under grant agreement No. 101093822, "SeaClear2.0".

parameter estimation to purely data-driven policies, reflects a fundamental shift in which data becomes the primary source of insight as complexity increases.

In recent years, operator-theoretic approaches have garnered substantial interest for learning nonlinear system dynamics from data (Kostic et al., 2022; Klus et al., 2020). Unlike conventional nonlinear representations in the physical state space, these methods describe the dynamics through a linear operator, most notably, the Koopman operator (Koopman, 1931), which fully characterizes the system’s evolution. This representational simplicity has enabled diverse applications including system identification (Li et al., 2017), soft robotics (Bruder et al., 2020), robust control (Strässer et al., 2023) and optimal control (Vaidya and Tellez-Castro, 2023; Caldarelli et al., 2025; Korda and Mezić, 2018).

Optimal control in state space traditionally relies on Bellman’s principle of optimality, but is severely limited by the curse of dimensionality, which renders Hamilton-Jacobi Bellman equations intractable even for moderate-scale problems (Bertsekas and Shreve, 1996). In such scenarios, local optimal control approaches, such as direct methods combined with sequential quadratic programming or interior points solvers (Diehl et al., 2009) have demonstrated superior performance over dynamic programming approaches. However, these local approaches require accurate initialization, are challenged by nonconvexity, and may result in suboptimal local solutions.

In contrast, convex reformulations offer a promising route to globally optimal solutions in nonlinear control via linear embedding methods (Vinter, 1993), sum-of-squares dual approaches (Henrion et al., 2008), or operator-theoretic system representations (Houska, 2025; Guo et al., 2022), each entailing fundamentally different algorithmic frameworks. Moreover, *convex* reformulations circumvent the linearization trade-offs inherent to traditional local methods. Operator-theoretic representations are particularly attractive as they can be learned from a single dataset by modern nonparametric operator-theoretic learning methods (Kostic et al., 2022, 2023; Bevanda et al., 2025a) and integrate naturally with stochastic control theory for diffusion processes (Fleming and Soner, 1993; Bogachev et al., 2015; Krylov, 2008). We therefore build on these techniques to address stochastic optimal control design in flexible, infinite-dimensional, Reproducing Kernel Hilbert Spaces (RKHSs), which have a rich history in machine learning (Steinwart and Christmann, 2008).

Contributions: This paper proposes a novel algorithm for solving data-driven stochastic optimal control problems. Our main contributions are:

1. We develop a nonparametric framework to learn finite-rank approximations of the Markov transition operators of stochastic control systems by using kernel regression techniques. The sample and time complexity of our kernel-based system identification method scales *linearly* with the number of states and controls.
2. We propose an RKHS embedded dynamic programming recursion, which leverages the data-driven Markov operator estimates to compute an associated approximation of the

global minimizer of stochastic optimal control problems.

The estimation and control algorithm is established under minimal system assumptions, without relying on stability conditions or detailed model knowledge, thereby relaxing common requirements in related existing works (Caldarelli et al., 2025; Vaidya and Tellez-Castro, 2023). In contrast to (Bevanda et al., 2025b), which relies on specific control excitations to learn infinitesimal generators, our method requires no such conditions, making it applicable to real-system data.

Organization: Section 2 reviews methods for reformulating stochastic optimal control problems as equivalent Partial Differential Equation (PDE) constrained optimization problems. Section 3 leverages empirical embeddings in an RKHS to introduce a data-driven approximation of the aforementioned optimal control problem. Finally, Section 4 applies the proposed method to benchmark optimal control problems.

Notation: We write $[n] := \{1, \dots, n\}$ for integers and \odot for the Hadamard product, \otimes for the tensor product; $\mathbb{X} = \mathbb{R}^{n_x}$ denotes the state space and $\mathbb{U} = \mathbb{R}^{n_u}$ the control space. The set of k -times continuously differentiable functions is denoted by $C^k(\mathbb{X})$, and $L^k(\mathbb{X})$ denotes the set of L^k -integrable functions. Additionally, $H^k(\mathbb{X})$ denotes the Hilbert-Sobolev space of k -times weakly differentiable functions on \mathbb{X} , including the special case $L^2(\mathbb{X}) = H^0(\mathbb{X})$. Generally, the dual Hilbert space of a Hilbert space H is denoted by H^* . As usual, $W(0, T; L^2(\mathbb{X}), H^1(\mathbb{X}))$ denotes the Bochner-Sobolev space of functions $\phi \in L^2(0, T; H^1(\mathbb{X}))$ whose weak time derivatives exist and satisfy $\dot{\phi} \in L^2(0, T; H^1(\mathbb{X})^*)$. With \mathcal{F} and \mathcal{Y} denoting separable Hilbert spaces, $\text{HS}(\mathcal{F}, \mathcal{Y})$ denotes the space of Hilbert–Schmidt operators with norm $\|A\|_{\text{HS}(\mathcal{F}, \mathcal{Y})}^2 := \sum_i \|Ae_i\|_{\mathcal{Y}}^2$ for any orthonormal basis $\{e_i\}$ of \mathcal{F} . Moreover, $\mathcal{Y} \otimes \mathcal{F}$ denotes the tensor product of Hilbert spaces. Whenever it is clear from the context which Hilbert space is meant, we write $\langle \cdot, \cdot \rangle$ for the inner product. Finally, “div” denotes the divergence and “ Δ ” the Laplacian.

1.1. Informal Problem Statement

Our goal is to find a *feedback control law* $\boldsymbol{\pi}$ solving the stochastic optimal control problem on the domain $\mathbb{X} = \mathbb{R}^{n_x}$

$$\lim_{T \rightarrow \infty} \min_{\boldsymbol{\pi} \in \Pi} \mathbb{E} \left[\int_0^T (\ell(\mathbf{X}_t) + r(\boldsymbol{\pi}_t(\mathbf{X}_t))) dt \right] \quad (1a)$$

$$\text{s.t. } d\mathbf{X}_t = (\mathbf{f}(\mathbf{X}_t) + \mathbf{G}(\mathbf{X}_t)\boldsymbol{\pi}_t(\mathbf{X}_t)) dt + \sqrt{2\epsilon} d\mathbf{W}_t, \quad (1b)$$

for *unknown* functions $(\mathbf{f}, \mathbf{G}, \ell)$ based on sampled measurements of the system states, inputs, and stage-cost rewards, $\{(\mathbf{x}_k, \mathbf{u}_k), \mathbf{x}_{k+1}, \ell(\mathbf{x}_k)\}$, corresponding to discrete-time observations of the Stochastic Differential Equation (SDE) (1b) under a small sampling time $h > 0$. Moreover, in this context, \mathbf{W}_t , $t \geq 0$, denotes a Wiener process and $\epsilon > 0$ a diffusion parameter. For brevity, we further introduce the notation

$$\Pi := L^\infty(0, T; \{\boldsymbol{\pi} \in L^\infty(\mathbb{X}) \mid \boldsymbol{\pi} \in \mathcal{U} \text{ on } \mathbb{X}\})$$

where the set $\mathcal{U} \subseteq \mathbb{R}^{n_u}$ models the control constraints.

We aim at a non-parametric and fully data-driven method that does not rely on prior knowledge about the system's properties and that

1. learns (1b) and the stage cost from snapshot data;
2. computes a data-driven approximation of the global minimizer of (1) in a computationally simple manner.

2. Stochastic Optimal Control

In this section, we introduce the stochastic optimal control problem formulation and briefly review select existing findings on the use of Fokker-Planck-Kolmogorov (FPK) operators for solving such problems through PDE-constrained optimization techniques (Crandall et al., 1992; Houska, 2025).

Assumption 1. *Throughout this paper, the following blanket assumptions are made.*

- (1) *The functions $\mathbf{f} \in C^1(\mathbb{X})^{n_x}$ and $\mathbf{G} \in C^1(\mathbb{X})^{n_x \times n_u}$ are continuously differentiable; and $\epsilon > 0$ is given.*
- (2) *The stage cost $\ell \in C^1(\mathbb{X})$ is continuously differentiable, bounded from below, and radially unbounded.*
- (3) *The initial state \mathbf{X}_0 is a random variable with given probability distribution $\rho_0 \in L^2(\mathbb{X})$.*
- (4) *The set $\mathcal{U} \subseteq \mathbb{R}^{n_u}$ is closed, convex, and $\text{int}(\mathcal{U}) \neq \emptyset$.*
- (5) *The control penalty $r \in C^1(\mathcal{U})$ is strongly convex.*
- (GC) *There exists a $\boldsymbol{\pi} : \mathbb{X} \rightarrow \text{int}(\mathcal{U})$, $\boldsymbol{\pi} \in L^\infty(\mathbb{X})$, a strongly convex $\mathcal{V} \in C^2(\mathbb{X})$ with bounded Hessian, and constants $C_1, C_2 < \infty$ such that*

$$(\mathbf{f}(\mathbf{x}) + \mathbf{G}(\mathbf{x})\boldsymbol{\pi}(\mathbf{x}))^\top \nabla \mathcal{V} \leq C_1 - C_2(\ell(\mathbf{x}) + r(\boldsymbol{\pi}(\mathbf{x})))$$

for all $\mathbf{x} \in \mathbb{X}$.

It is worth noting that conditions (1)-(5) of Assumption 1 are considered standard and typically do not impose restrictive limitations for practical applications. (GC) can be viewed as a growth constraint imposed on $\mathbf{f}, \mathbf{G}, \ell, r$ as \mathbf{x} tends to infinity. This criterion is often readily met in practical scenarios (Houska, 2025), as the constant C_1 can assume a potentially large positive value.

2.1. Fokker-Planck-Kolmogorov PDEs

As long as Assumption 1 holds, the martingale solution \mathbf{X}_t in (1b) constitutes a time-homogeneous Markov diffusion process whose transition operator, $\Gamma_t(\boldsymbol{\pi}) : L^2(\mathbb{X}) \rightarrow H^1(\mathbb{X})$, $t > 0$, maps the initial probability distribution $\rho_0 \in L^2(\mathbb{X})$ of \mathbf{X}_0 to the probability density function $\rho_t \in L^2(\mathbb{X})$ of \mathbf{X}_t ,

$$\forall t \in (0, T], \quad \rho_t = \Gamma_t(\boldsymbol{\pi})\rho_0.$$

Note that $\Gamma_t(\boldsymbol{\pi})$ is for any given $\boldsymbol{\pi} \in \mathcal{U}$ and any $t > 0$ a bounded linear operator on $H^1(\mathbb{X})$ (Hinze et al., 2009; Oksendal, 2000). Its associated differential generator is given by

$$\forall \rho \in C^\infty(\mathbb{X}), \quad \mathcal{L}(\boldsymbol{\pi})\rho := \lim_{t \rightarrow 0^+} \frac{\Gamma_t(\boldsymbol{\pi})\rho - \rho}{t}.$$

This operator is also known as the Fokker-Planck-Kolmogorov (FPK) operator (Bogachev et al., 2015). For differentiable feedback laws $\boldsymbol{\pi}$ and smooth test functions $\rho, V \in C^\infty(\mathbb{X})$, this operator is given by

$$\mathcal{L}(\boldsymbol{\pi})\rho = -\operatorname{div}(\rho(\mathbf{f} + \mathbf{G}\boldsymbol{\pi})) + \epsilon\Delta\rho \quad (2)$$

For the case that $\boldsymbol{\pi} \in \Pi$ is a potentially time-varying feedback law, the evolution of the probability density $\rho \in W(0, T; L^2(\mathbb{X}), H^1(\mathbb{X}))$ of the state of (1b) satisfies—if it exists—the parabolic FPK (Bogachev et al., 2015; Oksendal, 2000)

$$\begin{aligned} \dot{\rho}_t &= \mathcal{L}(\boldsymbol{\pi}_t)\rho_t = \mathcal{A}\rho_t + \mathcal{B}(\boldsymbol{\pi}_t\rho_t) \\ \text{with } \lim_{t \rightarrow 0^+} \rho_t &= \rho_0 \end{aligned} \quad (3)$$

in the weak sense. Note that $\mathcal{L}(\boldsymbol{\pi})$ is affine in $\boldsymbol{\pi}$. Hence, we define the time-autonomous operators \mathcal{A} and \mathcal{B} by $\mathcal{A}\rho = -\operatorname{div}(\mathbf{f}\rho) + \epsilon\Delta\rho$ and $\mathcal{B}(\boldsymbol{\pi}\rho) = -\operatorname{div}(\mathbf{G}\boldsymbol{\pi}\rho)$ for all test function $\rho \in C^\infty$.

If Assumption 1 holds and the horizon is finite ($T < \infty$), then for any time-invariant feedback law $\boldsymbol{\pi} \in \mathcal{U}$ satisfying the last condition of Assumption 1, a unique weak solution to (3) and a corresponding martingale solution \mathbf{X}_t of (1b) exist (Houska, 2025; Oksendal, 2000). In particular, the knowledge of a weak solution for at least one policy $\boldsymbol{\pi}$ suffices to guarantee strict feasibility of (1) (Houska, 2025).

2.2. Convex Reformulation

By using the notion of weak solutions of parabolic FPKs, the original stochastic optimal control problem (1) can be cast into a *convex* PDE-constrained optimization problem (Hinze et al., 2009; Houska, 2025), through a change of variables, $\boldsymbol{\nu} = \boldsymbol{\pi}\rho$,

$$\begin{aligned} \mathcal{J}(T, \rho_0) &:= \min_{\rho, \boldsymbol{\nu}} \int_0^T \int_{\mathbb{X}} \left(\ell + r \left(\frac{\boldsymbol{\nu}}{\rho} \right) \right) \rho \, d\mathbf{x} \, dt \\ \text{s.t. } &\begin{cases} \dot{\rho} = \mathcal{A}\rho + \mathcal{B}\boldsymbol{\nu} & \text{on } \mathbb{X}_T \\ \boldsymbol{\nu} \in \rho\mathcal{U} & \text{on } \mathbb{X}_T \\ \rho(0) = \rho_0 & \text{on } \mathbb{X}, \end{cases} \end{aligned} \quad (4)$$

with $\mathbb{X}_T = (0, T) \times \mathbb{X}$. Since $\epsilon > 0$, the density $\rho_t = \Gamma_{\boldsymbol{\pi}}(t)\rho_0$ satisfies $\rho_t > 0$ for $t > 0$, see (Bogachev et al., 2015).

Proposition 1 (Houska 2025, Thm. 1). *If Assumption 1 holds, (4) admits a unique minimizer $(\rho^*, \boldsymbol{\nu}^*)$ with*

$$\rho^* \in W(0, T; L^2(\mathbb{X}), H^1(\mathbb{X})) \text{ and } \boldsymbol{\nu}^* \in L^2(0, T; L^2(\mathbb{X})^{n_u}).$$

Moreover, the optimal feedback law is given by $\boldsymbol{\pi}^* = \frac{\boldsymbol{\nu}^*}{\rho^*}$ and $\rho^*(t)$ corresponds to the probability density of the optimal state \mathbf{X}_t^* .

Remark 1. If Assumption 1 holds,

$$\begin{aligned} \ell_\infty &= \min_{\rho_\infty, \nu_\infty} \int_{\mathbb{X}} \left(\ell + r \left(\frac{\nu_\infty}{\rho_\infty} \right) \right) \rho_\infty d\mathbf{x} dt \\ \text{s.t. } & \begin{cases} 0 = \mathcal{A}\rho_\infty + \mathcal{B}\nu_\infty & \text{on } \mathbb{X} \\ \nu_\infty \in \rho_\infty \mathcal{U} & \text{on } \mathbb{X} \\ 1 = \int_{\mathbb{X}} \rho_\infty dx \end{cases} \end{aligned} \quad (5)$$

has a unique minimizer $(\rho_\infty^*, \nu_\infty^*) \in H^1(\mathbb{X}) \times L^2(\mathbb{X})$, see (Houska, 2025, Cor. 1). Moreover, under the additional assumption that the stage cost ℓ has a finite variance for the steady-state density, $\int (\ell - \ell_\infty)^2 \rho_\infty dx < \infty$, we have

$$\ell_\infty = \lim_{T \rightarrow \infty} \frac{1}{T} \mathcal{J}(T, \rho_0).$$

Because ℓ_∞ is constant, it can be interpreted as an ergodic limit that does not depend on the initial density ρ_0 .

2.3. Hamilton-Jacobi-Bellman Equation

Let us now connect (4) to the well-known stochastic Hamilton-Jacobi-Bellman (HJB) equation (Fleming and Soner, 1993).

Let μ be the ergodic measure at steady-state, such that $d\mu = \rho_\infty dx$. Building on the strong duality based argument in (Houska, 2025, Theorem 2), we can construct a Riesz representation of the bounded linear operator

$$\mathcal{J}(T, \rho_0) = \int_{\mathbb{X}} V(0) \rho_0 dx,$$

where $V(0)$ is the initial value of a strongly measurable function $V : [0, T] \rightarrow H_\mu^1(\mathbb{X})$, which turns out to be the weak solution of the HJB equation

$$-\dot{V} = \mathcal{A}^* V + \ell + \min_{\pi \in \Pi} \{ r(\pi) + \pi^\top \mathcal{B}^* V \} \quad \text{on } (0, T) \times \mathbb{X} \quad (6)$$

with $V(T) = 0$ on \mathbb{X} , thereby enabling the explicit computation of optimal controls and the corresponding value function for the stochastic control problem.

2.4. Discretization of Time

This section introduces a discrete-time approximation of the bounded linear operator $\mathcal{J}(T, \cdot)$. For this aim, we choose a step-size $h > 0$ and define the discrete times $t_k = kh$ for $k \in \mathbb{N}$. By substituting a piecewise-constant approximation of the control law, $\pi(t, \mathbf{x}) = \pi_k(\mathbf{x})$, for $t \in [t_k, t_{k+1}]$, we arrive at the discrete-time approximation

$$\begin{aligned} \mathcal{J}_H(\rho_0) &:= \min_{\rho, \nu} \sum_{k=0}^{H-1} \int_{\mathbb{X}} \left(\ell_h + r_h \left(\frac{\nu_k}{\rho_k} \right) \right) \rho_k dx \\ \text{s.t. } & \begin{cases} \rho_{k+1} = \mathcal{A}\rho_k + \mathcal{B}\nu_k & \text{on } \mathbb{X} \\ \nu_k \in \rho_k \mathcal{U}, \end{cases} \end{aligned} \quad (7)$$

which is defined for all $\rho_0 \in L^2(\mathbb{X})$. Here, \mathbf{A} and \mathbf{B} denote the Hankel transition operators of the linear differential equation (3),

$$\mathbf{A} := \exp(\mathcal{A}h), \quad \mathbf{B} := \int_0^h \exp(\mathcal{A}\tau) \mathcal{B} d\tau. \quad (8)$$

Here, we define $\ell_h = h\ell$ and $r_h = hr$. If Assumption 1 holds, \mathbf{J}_H is again a bounded linear operator on $L^2(\mathbb{X})$ that admits a Riesz representation, $\mathbf{J}_H(\rho_0) = \int_{\mathbb{X}} V_0 \rho_0 dx$. By working out the corresponding dual problem, it turns out that V_0 can be found by solving the following operator-dynamic programming recursion

$$\begin{aligned} V_k &= \mathbf{A}^* V_{k+1} + \ell_h + \min_{\boldsymbol{\pi} \in \Pi} \{r_h(\boldsymbol{\pi}) + \boldsymbol{\pi}^\top \mathbf{B}^* V\} && \text{on } \mathbb{X}, \\ V_H &= 0 && \text{on } \mathbb{X}. \end{aligned} \quad (9)$$

which can be interpreted as a time-discretization of (6).

Remark 2. *For finite horizon optimal control problems, the above time-discretization leads to a discretization error, since the optimal density and control law are, in general, not time-invariant. Nevertheless, in the ergodic limit, we still have*

$$\ell_\infty = \lim_{T \rightarrow \infty} \frac{1}{T} \mathcal{J}(T, \rho_0) = \lim_{H \rightarrow \infty} \frac{1}{hH} \mathbf{J}_H(\rho_0)$$

for any $h > 0$ and any $\rho_0 \in L^2(\mathbb{X})$, because the ergodic feedback law, given by $\boldsymbol{\pi}_\infty = \frac{\nu_\infty}{\rho_\infty}$, is time-invariant.

3. OPTIMAL CONTROL MEETS RKHS EMBEDDINGS

The objective of this section is to propose a data-driven approach for approximating the solution of the stochastic optimal control problem.

3.1. Reproducing Kernel Hilbert Spaces

Reproducing Kernel Hilbert Spaces (RKHS) are widely accepted as the key to non-parametric statistical learning in function spaces (Steinwart and Christmann, 2008). Let $k : \mathbb{X} \times \mathbb{X} \rightarrow \mathbb{R}$ be a non-negative, symmetric, and continuous kernel and let $(\mathcal{H}_{\mathbb{X}}, \langle \cdot, \cdot \rangle_{\mathcal{H}_{\mathbb{X}}})$ be an associated RKHS. This means that $(\mathcal{H}_{\mathbb{X}}, \langle \cdot, \cdot \rangle_{\mathcal{H}_{\mathbb{X}}})$ is a Hilbert space, whose inner product satisfies the reproducing property $\psi(\mathbf{x}) = \langle k(\cdot, \mathbf{x}), \psi \rangle_{\mathcal{H}_{\mathbb{X}}}$ for all $\mathbf{x} \in \mathbb{X}$ and all observables $\psi \in \mathcal{H}_{\mathbb{X}}$. In the following, we assume that $\mathcal{H}_{\mathbb{X}}$ is a dense subspace of $H^1(\mathbb{X})$, k is universal¹, and $k(\mathbf{x}, \mathbf{x}') < \infty$ for all $\mathbf{x}, \mathbf{x}' \in \mathbb{X}$.

¹This is a property satisfied by many common kernels such as Gaussian and Matérn, see (Steinwart and Christmann, 2008).

3.2. RKHS Embeddings

We introduce the following embedding of a probability density $\rho \in L^2(\mathbb{X})$ into an RKHS $\mathcal{H}_{\mathbb{X}}$ as

$$\mathcal{E}_{\mathbb{X}} : L^2(\mathbb{X}) \rightarrow \mathcal{H}_{\mathbb{X}}, \quad \rho \rightarrow \int_{\mathbb{X}} k(\cdot, \mathbf{x}) \rho(\mathbf{x}) d\mathbf{x} \in \mathcal{H}_{\mathbb{X}} \quad (10)$$

It can be interpreted as the expected value of the feature map, namely $\mathcal{E}_{\mathbb{X}}\rho = \mathbb{E}_{\mathbf{X} \sim \rho}[k(\cdot, \mathbf{X})]$. Equivalently, $\mathcal{E}_{\mathbb{X}}$ can be viewed as the kernel mean embedding (KME) (Muandet et al., 2017) of the probability measure μ with density ρ with respect to the Lebesgue measure, $d\mu(\mathbf{x}) = \rho(\mathbf{x}) d\mathbf{x}$. We also define the embedding $\mathcal{E}_{\mathbb{X},U} : \mathbb{R}^{n_u} \rightarrow \mathbb{R}^{n_u} \otimes \mathcal{H}_{\mathbb{X}}$ of the controls $\boldsymbol{\nu} \in L^2(\mathbb{X}, \mathbb{R}^{n_u})$ into an RKHS $\mathbb{R}^{n_u} \otimes \mathcal{H}_{\mathbb{X}}$ by

$$\mathcal{E}_{\mathbb{X},U} \boldsymbol{\nu} := \int_{\mathbb{X}} \boldsymbol{\nu}(\mathbf{x}) \otimes k(\cdot, \mathbf{x}) d\mathbf{x} \in \mathbb{R}^{n_u} \otimes \mathcal{H}_{\mathbb{X}}. \quad (11)$$

Next, we embed and approximate the dynamics in (7) as

$$\mathcal{E}_{\mathbb{X}}\rho_{k+1} = \mathcal{E}_{\mathbb{X}}(\mathbf{A}\rho_k + \mathbf{B}\boldsymbol{\nu}_k) \approx A\mathcal{E}_{\mathbb{X}}\rho_k + B\mathcal{E}_{\mathbb{X},U}\boldsymbol{\nu}_k, \quad (12)$$

where $A \in \text{HS}(\mathcal{H}_{\mathbb{X}}, \mathcal{H}_{\mathbb{X}})$ and $B \in \text{HS}(\mathbb{R}^{n_u} \otimes \mathcal{H}_{\mathbb{X}}, \mathcal{H}_{\mathbb{X}})$, are RKHS approximations of (\mathbf{A}, \mathbf{B}) , which we will learn from data in the next paragraph.

3.3. Data-Driven Operator Learning

In practice, we do not have access to population (infinite data) levels to work directly with the embeddings introduced previously. However, we assume the existence of (finite) training samples of the form

$$\mathbb{D}_n = \{(\mathbf{x}^{(i)}, \mathbf{u}^{(i)}), \mathbf{x}_+^{(i)}, \ell(\mathbf{x}^{(i)})\}_{i \in [n]}, \quad (13)$$

where the states and controls are selected according to a strictly positive probability measure $\mu \in M_+^1(\mathbb{X} \times \mathbb{U})$. Note that the stage cost values $\ell(\mathbf{x}^{(i)})$ may either be sampled (as shown) or computed directly if ℓ is known a priori.

We define the dataset-dependent empirical embeddings $\widehat{\mathcal{E}}_{\mathbb{X}}, \widehat{\mathcal{E}}_+ : \mathbb{R}^n \rightarrow \mathcal{H}_{\mathbb{X}}$ and $\widehat{\mathcal{E}}_{\mathbb{X},U} : \mathbb{R}^n \rightarrow \mathbb{R}^{n_u} \otimes \mathcal{H}_{\mathbb{X}}$ by

$$\widehat{\mathcal{E}}_{\mathbb{X}}\mathbf{w} := \frac{1}{\sqrt{n}} \sum_{i=1}^n w_i k(\cdot, \mathbf{x}^{(i)}), \quad (14)$$

$$\widehat{\mathcal{E}}_+\mathbf{w} := \frac{1}{\sqrt{n}} \sum_{i=1}^n w_i k(\cdot, \mathbf{x}_+^{(i)}), \quad (15)$$

$$\widehat{\mathcal{E}}_{\mathbb{X},U}\mathbf{w} := \frac{1}{\sqrt{n}} \sum_{i=1}^n w_i \mathbf{u}^{(i)} \otimes k(\cdot, \mathbf{x}^{(i)}) \quad (16)$$

for all $\mathbf{w} \in \mathbb{R}^n$. Let $\mathbb{R}^n = \text{span}\{\mathbf{e}_i\}_{i=1}^n$ denote a canonical basis. By substituting the empirical embeddings (14)-(16) in (12), we can write the empirical residual as

$$\hat{r}_i = (\widehat{\mathcal{E}}_+ - (A\widehat{\mathcal{E}}_{\mathbb{X}} + B\widehat{\mathcal{E}}_{\mathbb{X},U}))\mathbf{e}_i \quad (17)$$

$$= \frac{1}{\sqrt{n}} (k(\cdot, \mathbf{x}_+^{(i)}) - (A k(\cdot, \mathbf{x}^{(i)}) + B(\mathbf{u}^{(i)} \otimes k(\cdot, \mathbf{x}^{(i)})))) \quad (18)$$

$$= \frac{1}{\sqrt{n}} k(\cdot, \mathbf{x}_+^{(i)}) - \frac{1}{\sqrt{n}} T([\frac{1}{\mathbf{u}}] \otimes k(\cdot, \mathbf{x}^{(i)})), \quad (19)$$

where we defined the operator $T \in \text{HS}(\mathcal{H}_{\mathbb{Z}}, \mathcal{H}_{\mathbb{X}})$, with the RKHS $\mathcal{H}_{\mathbb{Z}} = \mathcal{H}_{\mathbb{X}} \oplus (\mathbb{R}^{n_u} \otimes \mathcal{H}_{\mathbb{X}})$. For brevity, we also introduce the shorthand $\mathbf{z} := [\begin{smallmatrix} \mathbf{x} \\ \mathbf{u} \end{smallmatrix}]$ so that $\mathbb{Z} := \mathbb{X} \times \mathbb{U}$.

Given the training samples (13), we can obtain an estimator (Muandet et al., 2017) by minimizing the squared RKHS norm error

$$\sum_{i=1}^n \|\hat{r}_i(T)\|_{\mathcal{H}_{\mathbb{X}}}^2 = \frac{1}{n} \sum_{i=1}^n \|k(\cdot, \mathbf{x}_+^{(i)}) - T([\begin{smallmatrix} 1 \\ \mathbf{u}^{(i)} \end{smallmatrix}] \otimes k(\cdot, \mathbf{x}^{(i)}))\|_{\mathcal{H}_{\mathbb{X}}}^2$$

over the residuals by solving

$$\hat{T} = \arg \min_{T \in \text{HS}(\mathcal{H}_{\mathbb{Z}}, \mathcal{H}_{\mathbb{X}})} \sum_{i=1}^n \|\hat{r}_i(T)\|_{\mathcal{H}_{\mathbb{X}}}^2 + \gamma \|T\|_{\text{HS}}^2, \quad (20)$$

where γ is a regularization, which ensures numerical stability and prevents overfitting. In addition to (14)-(16), we introduce the sampling operators

$$\hat{\mathcal{E}}_{\mathbb{Z}}^* : \mathcal{H}_{\mathbb{Z}} \rightarrow \mathbb{R}^n, \quad \hat{\mathcal{E}}_{\mathbb{Z}}^* k_{\mathbb{Z}}(\cdot, \mathbf{z}) = \frac{1}{\sqrt{n}} [k_{\mathbb{Z}}(\mathbf{z}, \mathbf{z}^{(i)})]_{i \in [n]}, \quad (21)$$

$$\hat{\mathcal{E}}_+^* : \mathcal{H}_{\mathbb{X}} \rightarrow \mathbb{R}^n, \quad \hat{\mathcal{E}}_+^* k(\cdot, \mathbf{x}) = \frac{1}{\sqrt{n}} [k(\mathbf{x}, \mathbf{x}_+^{(i)})]_{i \in [n]}, \quad (22)$$

where $k_{\mathbb{Z}}(\mathbf{z}, \mathbf{z}') = k(\mathbf{x}', \mathbf{x})(1 + \langle \mathbf{u}, \mathbf{u}' \rangle)$, see (Bevanda et al., 2025a). Note that the above sampling operators are the adjoints of the corresponding empirical embeddings $\hat{\mathcal{E}}_{\mathbb{Z}}$ and $\hat{\mathcal{E}}_+$. Applying the kernel trick, we can obtain the Gram matrices $(\hat{\mathcal{E}}_{\mathbb{X}}^* \hat{\mathcal{E}}_{\mathbb{X}})_{ij} := (\mathbf{K}_{\mathbb{X}})_{ij} = \frac{1}{n} k(\mathbf{x}^{(i)}, \mathbf{x}^{(j)})$ and $(\hat{\mathcal{E}}_{\mathbb{Z}}^* \hat{\mathcal{E}}_{\mathbb{Z}})_{ij} := (\mathbf{K})_{ij} = \frac{1}{n} k_{\mathbb{Z}}(\mathbf{z}^{(i)}, \mathbf{z}^{(j)})$. The regularized inverse of this Gram matrix is denoted by $\mathbf{K}_{\gamma}^{-1} = (\hat{\mathcal{E}}_{\mathbb{Z}}^* \hat{\mathcal{E}}_{\mathbb{Z}} + \gamma \mathbf{I})^{-1} = (\mathbf{K} + \gamma \mathbf{I})^{-1}$, defining the solution to (20) as $\hat{T} = \hat{\mathcal{E}}_+ \mathbf{K}_{\gamma}^{-1} \hat{\mathcal{E}}_{\mathbb{Z}}^*$. This, in turn, reads

$$\hat{T} = [\hat{A} \quad \hat{B}] = [\hat{\mathcal{E}}_+ \mathbf{K}_{\gamma}^{-1} \hat{\mathcal{E}}_{\mathbb{X}}^* \quad \hat{\mathcal{E}}_+ \mathbf{K}_{\gamma}^{-1} \hat{\mathcal{E}}_{\mathbb{X}, \mathbb{U}}^*], \quad (23)$$

which is dual to learning control Koopman Operators (cKOR) in (Bevanda et al., 2025a).

The regression formulation above resembles the Extended Dynamic Mode Decomposition (EDMD) framework (Williams et al., 2015), but uses feature maps in an RKHS instead of an explicit observable dictionary. This obviates the need for explicit tensor products between the dictionary and controls (Strässer et al., 2023). Furthermore, with universal kernels, the resulting kernel methods allow arbitrarily accurate learning of these operators.

3.4. DATA-DRIVEN OPTIMAL CONTROL

In this section, we aim to develop a data-driven approximation of (9), using the estimators \hat{A}, \hat{B} from the previous section. Recall that the Riesz representer V_0 is obtained as the (weak) solution of the discretized stochastic HJB equation in (9). Let us define the Fenchel conjugate

$$D_r(\boldsymbol{\lambda}) := \min_{\mathbf{u} \in \mathcal{U}} \{r_h(\mathbf{u}) + \boldsymbol{\lambda}^\top \mathbf{u}\} \quad (24)$$

$$\text{with } \mathbf{u}^*(\boldsymbol{\lambda}) := \arg \min_{\mathbf{u} \in \mathcal{U}} \{r_h(\mathbf{u}) + \boldsymbol{\lambda}^\top \mathbf{u}\}, \quad (25)$$

where, as in (9), we set $r_h = hr$. Since we assume that r is strongly convex, while \mathcal{U} is compact, convex, and has a non-empty interior, the parametric minimizer \mathbf{u}^* is unique and Lipschitz continuous. To derive a surrogate of (9) in the RKHS $\mathcal{H}_{\mathbb{X}}$, we provide the cost $\ell_h = h\ell$ and the Fenchel conjugate D_r representations via $\widehat{\mathcal{E}}_{\mathbb{X}}$ (14)

$$\widehat{\ell}_h := \widehat{\mathcal{E}}_{\mathbb{X}} \ell_h, \quad \widehat{D}_r(\cdot) := \widehat{\mathcal{E}}_{\mathbb{X}} \mathbf{D}_r(\cdot),$$

respectively, where $\mathbf{D}_r(\cdot) : \mathbb{R}^{nnu} \rightarrow \mathbb{R}^n$ and $\ell_h \in \mathbb{R}^n$. Substituting the adjoints of the learned operator model $(\widehat{A}, \widehat{B})$ from (23) into (9) then yields the following RKHS embedded dynamic programming recursion for $\widehat{V}_k \in \mathcal{H}_{\mathbb{X}}$

$$\widehat{V}_k = \widehat{A}^* \widehat{V}_{k+1} + \widehat{\ell}_h + \widehat{D}_r(\widehat{B}^* \widehat{V}_{k+1}), \quad \widehat{V}_H = 0, \quad (26)$$

where $h > 0$ and H denote the discrete-time step and horizon, respectively. While (26) is intractable in this form, under the finite-data setting (13) we obtain finite-rank \widehat{A} and \widehat{B} in (23). Next, we insert their adjoints $(\widehat{A}^*, \widehat{B}^*)$ into (26) and test \widehat{V}_k against $k(\cdot, \mathbf{x})$, which yields

$$\langle \widehat{A}k(\cdot, \mathbf{x}), \widehat{V}_0 \rangle_{\mathcal{H}_{\mathbb{X}}} = \langle \widehat{\mathcal{E}}_{\mathbb{X}}^* k(\cdot, \mathbf{x}), \mathbf{K}_{\gamma}^{-1} \mathbf{K}_+ \mathbf{v}_0 \rangle_{\mathbb{R}^n} = \langle \mathbf{k}(\mathbf{x}), \mathbf{A} \mathbf{v}_0 \rangle_{\mathbb{R}^n}$$

with $(\mathbf{K}_+)^{ij} = (\widehat{\mathcal{E}}_+^* \widehat{\mathcal{E}}_{\mathbb{X}})^{ij} = k(\mathbf{x}_+^{(i)}, \mathbf{x}^{(j)})$ and

$$\langle \widehat{B}(\mathbf{u} \otimes k(\cdot, \mathbf{x})), \widehat{V}_0 \rangle_{\mathcal{H}_{\mathbb{X}}} = \langle \text{diag}(\mathbf{U} \mathbf{u}) \mathbf{k}(\mathbf{x}), \mathbf{A} \mathbf{v}_0 \rangle_{\mathbb{R}^n},$$

where we used $\widehat{\mathcal{E}}_{\mathbb{X}, \mathbf{U}}^*(\mathbf{u} \otimes k(\cdot, \mathbf{x})) = \text{diag}(\mathbf{U} \mathbf{u}) \mathbf{k}(\mathbf{x})$. Thus, we obtain *tractable* matrix representations

$$\mathbf{A} = \mathbf{K}_{\gamma}^{-1} \mathbf{K}_+, \quad \mathbf{B} = [\text{diag}(\mathbf{U} \mathbf{e}_i) \mathbf{K}_{\gamma}^{-1} \mathbf{K}_+]_{i \in [n_u]}. \quad (27)$$

Additionally, we define the RKHS representations

$$\widehat{\ell}_h := \widehat{\mathcal{E}}_{\mathbb{X}} \ell_h, \quad \widehat{D}_r(\widehat{B}^* \widehat{V}_{k+1}) := \widehat{\mathcal{E}}_{\mathbb{X}} \mathbf{D}_r(\mathbf{B} \mathbf{v}_{k+1}), \quad (28)$$

where $\mathbf{D}_r(\mathbf{B} \mathbf{v}_{k+1}) = \mathbf{K}_{\gamma}^{-1} [\mathbf{D}_r([\widehat{B}^* \widehat{V}_{k+1}](\mathbf{x}^{(i)}))]_{i \in [n]}$ and $\ell_h = \mathbf{K}_{\gamma}^{-1} [\ell_h^{(i)}]_{i \in [n]}$ are the Kernel Ridge Regression (KRR) solutions corresponding to the evaluated dual terms on the dataset (13) and the sampled stage costs, respectively. Since elements of $\mathbb{R}^{nnu} \otimes \mathcal{H}_{\mathbb{X}}$ are equivalent to $\mathcal{H}_{\mathbb{X}}^{nnu}$, $[\widehat{B}^* \widehat{V}_{k+1}](\mathbf{x}^{(i)}) = \langle \mathbf{I}_{n_u} \otimes \mathbf{k}(\mathbf{x}^{(i)}), \mathbf{B} \mathbf{v}_{k+1} \rangle_{\mathbb{R}^{nnu}}$. Those derivations lead to an exact and tractable recursion with matrix representations, as detailed in the following result.

Theorem 1. *Let \widehat{A}, \widehat{B} be the estimators in (23), and define $\widehat{\ell}_h$ and $\widehat{D}_r(\widehat{B}^* \widehat{V}_{k+1})$ as in (28). Then the operator recursion (26) evolves in a finite- n -dimensional subspace, and is equivalent to the Kernel HJB (KHJB) recursion*

$$\begin{aligned} \mathbf{v}_k &= \mathbf{A} \mathbf{v}_{k+1} + \ell_h + \mathbf{D}_r(\mathbf{B} \mathbf{v}_{k+1}) \\ \text{s.t. } \mathbf{v}_H &= \mathbf{0} \end{aligned} \quad (29)$$

with $\mathbf{v}_k \in \mathbb{R}^n$ and matrices (\mathbf{A}, \mathbf{B}) given in (27).

Table 1: Computational complexity of Algorithm 1.

Task	Complexity
Regression	$\mathcal{O}(n^3 + n^2(n_x + n_u))$
Control (KHJB)	$\mathcal{O}(H(n^2 n_u + n n_u^2))$

Proof. This statement follows from the finite-rank representation for \widehat{A}, \widehat{B} . The first step to obtain (29) consists in writing the empirical embedding $\widehat{V}_k = \widehat{\mathcal{E}}_{\mathcal{X}} \mathbf{v}_k$ and leverage the reproducing property $\widehat{V}_k(\mathbf{x}) = \langle k(\cdot, \mathbf{x}), \widehat{V}_k \rangle = \langle \mathcal{E}_{\mathcal{X}}^* k(\cdot, \mathbf{x}), \mathbf{v}_k \rangle = \langle \mathbf{k}(\mathbf{x}), \mathbf{v}_k \rangle$ with the sampled canonical feature map $\mathbf{k}(\mathbf{x}) = \frac{1}{\sqrt{n}} [k(\mathbf{x}, \mathbf{x}^{(i)})]_{i \in [n]}$. Then (29) follows directly from substituting $(\widehat{A}^*, \widehat{B}^*)$ along with (28) in (26). \square \square

We call the recursion (29) starting at \mathbf{v}_H the discrete-time KHJB, because it can be interpreted as a discretized version of the original HJB (6), for $T = Hh$. It can be used to approximate the (true) optimal value function V^* —that is, the optimal co-state of (4)—via the reproducing property $\widehat{V}^*(\mathbf{x}) = \langle \mathbf{k}(\mathbf{x}), \mathbf{v}_0 \rangle$.

This approximation introduces two main sources of error: the *discretization error* and the *learning error* incurred during the estimation of the operator model in (23). Note that for the latter, under standard regularity assumptions and using universal kernels, the data-driven estimators of the operators in (23) are consistent and converge to the true operators in the data limit; see (Kostic et al., 2023). A more in-depth error analysis, however, is beyond the scope of this work.

To return to our problem formulation and the objective of finding an optimal feedback control law $\boldsymbol{\pi}^*$ minimizing the ergodic cost in the SOCP (1), an approximate solution can be readily obtained as

$$\widehat{\boldsymbol{\pi}}^*(\mathbf{x}) = \mathbf{u}^* (\langle \mathbf{I}_{n_u} \otimes \mathbf{k}(\mathbf{x}), \mathbf{B} \mathbf{v}^* \rangle_{\mathbb{R}^{n n_u}}). \quad (30)$$

4. Implementation and Numerical Examples

4.1. The KHJB Algorithm

The implementation follows Algorithm 1, with its computational complexity summarized in Table 1. The main bottleneck is the inversion of the $n \times n$ matrix defining \mathbf{K}_γ^{-1} , which scales as $\mathcal{O}(n^3)$. Each control-update step requires evaluating the Fenchel conjugate of the control penalty ($\mathcal{O}(n_u^2)$) and computing $\mathbf{B} \mathbf{v}$ ($\mathcal{O}(n^2 n_u)$). It is also worth noting that the complexity scales *linearly* with the state dimensionality n_x .

4.2. Numerical Examples

In this section, we present numerical examples implemented in **Julia** to evaluate the accuracy of the data-driven generated global optimal control law using Algorithm 1.

Algorithm 1 Nonparametric Optimal Control

Require: Data \mathbb{D}_n (13), minimizer $\mathbf{u}^*(\cdot)$ (25), kernel k , horizon H and sampling time $h > 0$; regularization parameter $\gamma > 0$, tolerance $\text{tol} > 0$.

Set $\mathbf{U} := [\mathbf{u}^{(1)}, \dots, \mathbf{u}^{(n)}]^\top$

Set $\mathbf{k}(\mathbf{x}) = [k(\mathbf{x}, \mathbf{x}^{(i)})]_{i \in [n]}$ $\triangleright \mathbf{k}(\mathbf{x}) \in \mathbb{R}^n$

/ Nonparametric Model Learning */*

Compute $(\mathbf{K}_X)_{ij} := k(\mathbf{x}^{(i)}, \mathbf{x}^{(j)})$

Compute $(\mathbf{K}_+)_{ij} := k(\mathbf{x}_+^{(i)}, \mathbf{x}^{(j)})$

Compute $\mathbf{K}_\gamma^{-1} := (\mathbf{K}_X + \mathbf{K}_X \odot \mathbf{U} \mathbf{U}^\top + \gamma \mathbf{I})^{-1}$

Compute $\mathbf{A} = \mathbf{K}_\gamma^{-1} \mathbf{K}_+$

Compute $\mathbf{B} = [\text{diag}(\mathbf{U} \mathbf{e}_i) \mathbf{A}]_{i \in [n_u]}$

/ Optimal Control (KHJB) */*

Set $D_r(\boldsymbol{\lambda}) = r(\mathbf{u}^*(\boldsymbol{\lambda}))h + \boldsymbol{\lambda}^\top \mathbf{u}^*(\boldsymbol{\lambda})$

$\boldsymbol{\lambda}(\mathbf{x}^{(i)}) = \langle \mathbf{I}_{n_u} \otimes \mathbf{k}(\mathbf{x}^{(i)}), \boldsymbol{\lambda} \rangle \in \mathbb{R}^{n_u}$ $\triangleright \boldsymbol{\lambda} \in \mathbb{R}^{nn_u}$

Set $\mathbf{D}_r(\boldsymbol{\lambda}) = \mathbf{K}_\gamma^{-1} [D_r(\boldsymbol{\lambda}(\mathbf{x}^{(i)}))]_{i \in [n]}$

Compute $\boldsymbol{\ell}_h = h \mathbf{K}_\gamma^{-1} [\ell(\mathbf{x}^{(i)})]_{i \in [n]}$

Set $\mathbf{v}_H \leftarrow \mathbf{0}$, $k \leftarrow H$

repeat

$\mathbf{v}_{k-1} = \mathbf{A} \mathbf{v}_k + \boldsymbol{\ell}_h + \mathbf{D}_r(\mathbf{B} \mathbf{v}_k)$

$k \leftarrow k - 1$

until $k = 0$ or $\|\mathbf{v}_k - \mathbf{v}_{k+1}\| \leq \text{tol}$

v^{*} = \mathbf{v}_k

output

$\widehat{V}^*(\mathbf{x}) = \mathbf{k}(\mathbf{x})^\top \mathbf{v}^*$ and $\widehat{\pi}^*(\mathbf{x}) = \mathbf{u}^*(\langle \mathbf{I}_{n_u} \otimes \mathbf{k}(\mathbf{x}), \mathbf{B} \mathbf{v}^* \rangle)$

Our numerical examples are based on Radial Basis Function (RBF) kernels of the form $k(\mathbf{x}, \mathbf{y}) = \exp(-\|\mathbf{x} - \mathbf{y}\|^2/\sigma^2)$. The RBF scale σ is tuned separately for each benchmark, using a grid search based on the prediction performance. For the 1D and 2D examples, we set $\gamma = 10^{-8}$ and $\epsilon = 0.02$ and collect data a uniform random scalar input u on the domain $\mathbb{U} = [-1, 1]$.

4.2.1. 1D Benchmark Collection

Let us consider the open-loop controlled scalar system $\dot{x} = f(x) + G(x)u$ with input $u \in \mathbb{R}$. For $f(x) = -\frac{1}{2}x(1 - G(x)^2)$ and stage cost functionals $\ell(x) = x^2$, $r(u) = u^2$, the globally optimal feedback control law is known and given by $\pi^*(x) = -G(x)x$ (Doyle et al., 1996). To obtain control laws with diverse characteristics, we implement three different instances of $G(x)$, listed as Systems S1, S2, and S3 in Table 2. Additionally, we implement another nonlinear system, System S4, with dynamics $\dot{x} = -x^3 + u$, for which the optimal control law has a known closed-form solution $\pi^*(x) = x^3 - x\sqrt{1 + x^4}$ (Guo et al., 2022). We generate 50 independent KRR estimations using $n = 1000$ training points for Systems S1, S2, and S3, and $n = 400$ points for System S4. Algorithm 1 runs for $H = 5000$ steps with sampling time

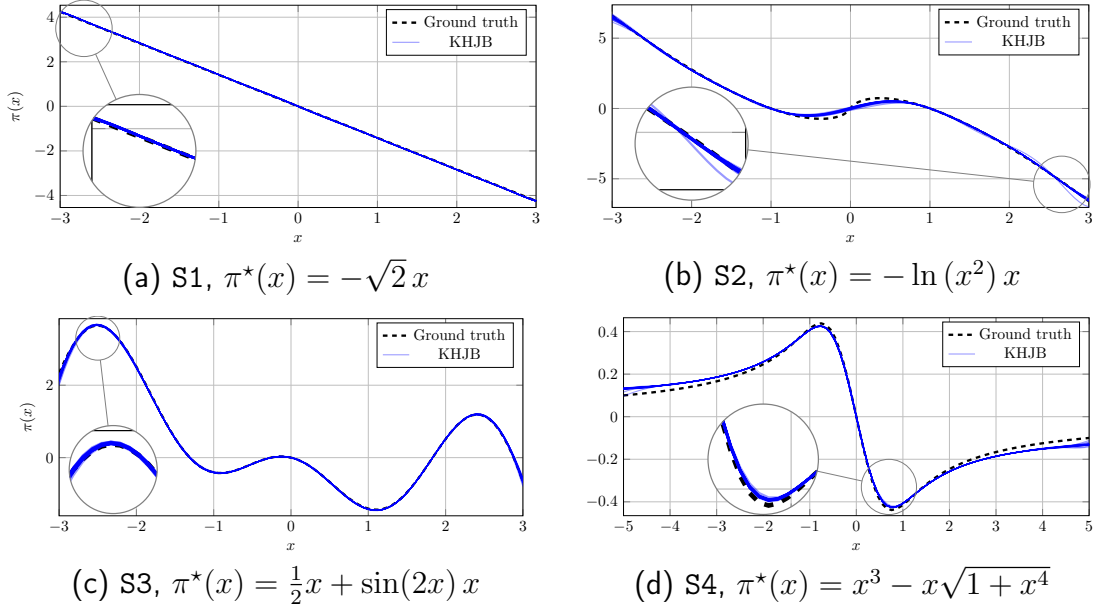


Figure 1: The optimal control laws π_∞^* for $\ell(x) = x^2$ and $r(u) = u^2$ are unknown to the algorithm but are used by us as ground truth. Our proposed data-driven Kernel HJB approach recovers these optimal control laws reliably and exhibits little variance across different i.i.d. data draws.

Table 2: Definitions of f and G for 1D benchmarks with the respective domain \mathbb{X}_S and sampling time h of the data.

System (\mathbb{X}_S, h)	$G(x)$	$f(x)$
S1 $([-3, 3], 10^{-2})$	$\sqrt{2}$	$\frac{1}{2}x$
S2 $([-3, 3], 10^{-3})$	$\ln(x^2)$	$-\frac{1}{2}x(1 - \ln(x^2)^2)$
S3 $([-3, 3], 10^{-3})$	$\frac{1}{2} + \sin(2x)$	$-\frac{3}{8}x + \frac{1}{2}x \sin(2x) + \frac{1}{2}x \sin(2x)^2$
S4 $([-5, 5], 10^{-2})$	1	$-x^3$

$h = 10^{-3}$ s, and $H = 500$ steps with $h = 10^{-2}$ s to ensure value function convergence. Figure 1 compares the control laws from Algorithm 1 against the known optimal controls.

Table 3 reports the mean and standard deviation of the Root Mean Squared Error (RMSE) $(n^{-1} \sum_{i=1}^n (\hat{\pi}^*(\mathbf{x}^{(i)}) - \pi^*(\mathbf{x}^{(i)}))^2)^{1/2}$ between estimated and optimal control laws. The systems, along with their respective domains and sampling times, are detailed in Table 2.

4.2.2. 2D-Unstable oscillator

Consider a Van der Pol oscillator system $\dot{x}_1 = x_2$, $\dot{x}_2 = -x_1 - \frac{1}{2}x_2(1 - x_1^2) + x_1u$ with stage cost $\ell(\mathbf{x}) = \frac{1}{2}x_2^2$, $r(u) = \frac{1}{2}u^2$. This system admits an explicit solution to the Hamilton-Jacobi-Bellman equations with globally optimal feedback law $\pi^*(\mathbf{x}) = -x_1x_2$ (Doyle et al., 1996). The system has a linearly uncontrollable equilibrium at $(0, 0)^\top$ and an unstable limit cycle (Figure 3, left). We sample $n = 2500$ training points from a grid with $|x_1| \leq 3$ and

Table 3: 1D-benchmarks: RMSE of the obtained control law versus the ground-truth control law, over 100 test datapoints.

System	RBF Scale σ	RMSE (mean)	RMSE (std)
S1	1.2	1.29×10^{-2}	1.59×10^{-3}
S2	1.8	1.31×10^{-1}	1.53×10^{-1}
S3	2	2.17×10^{-2}	8.13×10^{-3}
S4	1	1.91×10^{-2}	2.94×10^{-4}

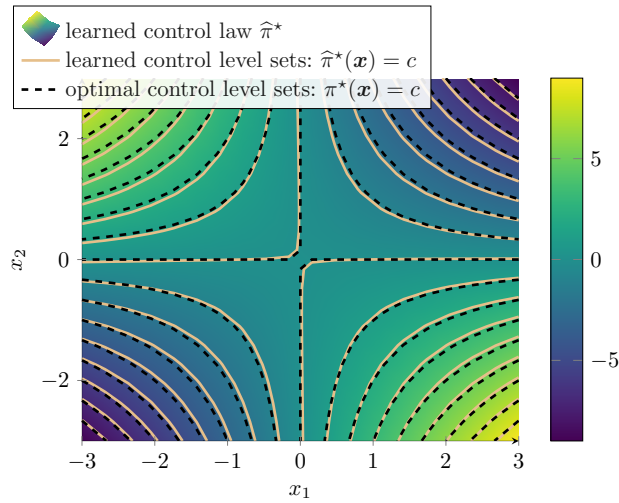


Figure 2: Contours of the learned optimal controller for the Van der Pol system, compared to the known optimal feedback law $\pi^*(\mathbf{x}) = -x_1 x_2$.

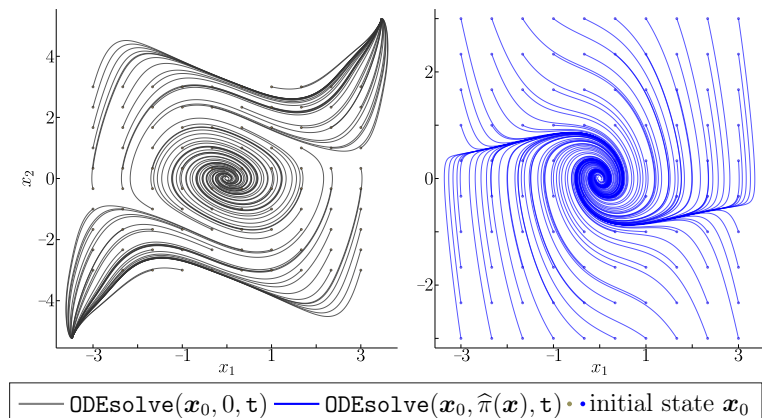


Figure 3: Taming an unstable limit cycling system with linearly uncontrollable origin. **Left:** Open loop ($u=0$) of the original system. **Right:** Closed loop under our learned control law for the stage cost $\ell(\mathbf{x})=x_2^2$.

$|x_2| \leq 3$ for KRR estimation using RBF scale $\sigma = 20$. Figure 2 shows the approximated feedback law closely matches the optimal $\pi^*(\mathbf{x})$, with RMSE 7.24×10^{-2} on 900 test points. Under the approximated feedback law, the closed-loop system exhibits an asymptotically stable origin (Figure 3, right).

4.2.3. 4D-Nonlinear AUV

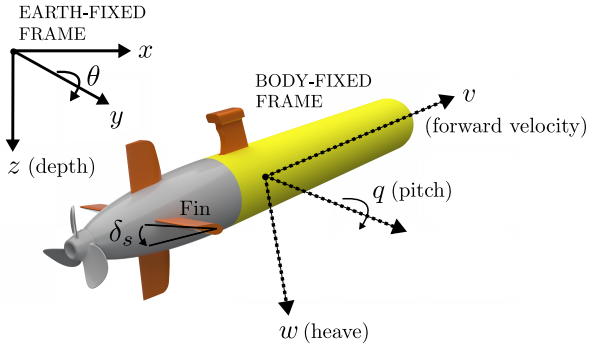


Figure 4: Autonomous Underwater Vehicle (AUV) model.

We consider depth control of an autonomous underwater vehicle (AUV) depicted in Figure 4 with constant forward velocity $v = 2\text{m/s}$ in a vertical plane. The state vector $\mathbf{x} = [w, q, z, \theta]^\top \in \mathbb{R}^4$ represents heave velocity (m/s), pitch rate (rad/s), depth (m), and pitch angle (rad), with control input δ_s denoting the fin deflection angle. We use the nonlinear model and parameters from (Naik and Singh, 2007), sampling $n = 8000$ i.i.d. training points within $[-0.5, 0.5] \times [-\pi/6, \pi/6] \times [0, 4] \times [-\pi/6, \pi/6]$ with random inputs $u \in [\pi/6, -\pi/6]$, collected at a sample rate of $h = 0.5\text{s}$. Moreover, we identify $\sigma = 35$ as the ideal RBF bandwidth and set $\epsilon = 0.001$ and $\gamma = 10^{-8}$. For a given depth reference z_{ref} , the state reference is set as $\mathbf{x}_{\text{ref}} = [0, 0, z_{\text{ref}}, 0]^\top$, with quadratic costs $\ell(\mathbf{x}) = (\mathbf{x} - \mathbf{x}_{\text{ref}})^\top Q(\mathbf{x} - \mathbf{x}_{\text{ref}})$ and $r(u) = u^\top R u$, where $Q = \text{diag}(100, 500, 100, 350) + Q_{\text{offdiag}}$ with $(Q_{\text{offdiag}})_{1,4} = (Q_{\text{offdiag}})_{4,1} = 500$ and $R = 50$. The RKHS embedded dynamic programming recursion is executed for $H = 1000$ steps with a hard constraint on the fin deflection angle, $|\delta_s| \leq 0.4363$ rad ($\pm 25^\circ$), to obtain a practical control law (Naik and Singh, 2007). We then evaluate the learned control law on the depth-tracking task² as shown in Figure 5 for a simulation time of $T = 50\text{s}$ and $M = 50$ runs.

As the vertical plane model (Naik and Singh, 2007) is made to enable linear control design in state-space for nonlinear systems, we implement a linear quadratic regulator (LQR), which uses the same cost matrices Q and R , and evaluate its performance over the M simulation runs. We compute the accumulated costs $J = \sum_{i=1}^M \int_0^T \ell(\mathbf{x}^{(i)}) + r(u^{(i)}) \, dt$ over the trajectories in Figure 5 for both approaches and find that our learned control law $\hat{\pi}$ achieves a mean cost reduction of 5.09% and a standard deviation reduction of 30.11% compared to the LQR baseline. The LQR controller, although derived from a linearized model, benefits from

²The same feedback can track a new reference z'_{ref} by exploiting the translation invariance of depth in the model of Naik and Singh (2007), redefining $\pi^*(\mathbf{x} - [0, 0, z'_{\text{ref}} - z_{\text{ref}}, 0]^\top)$.

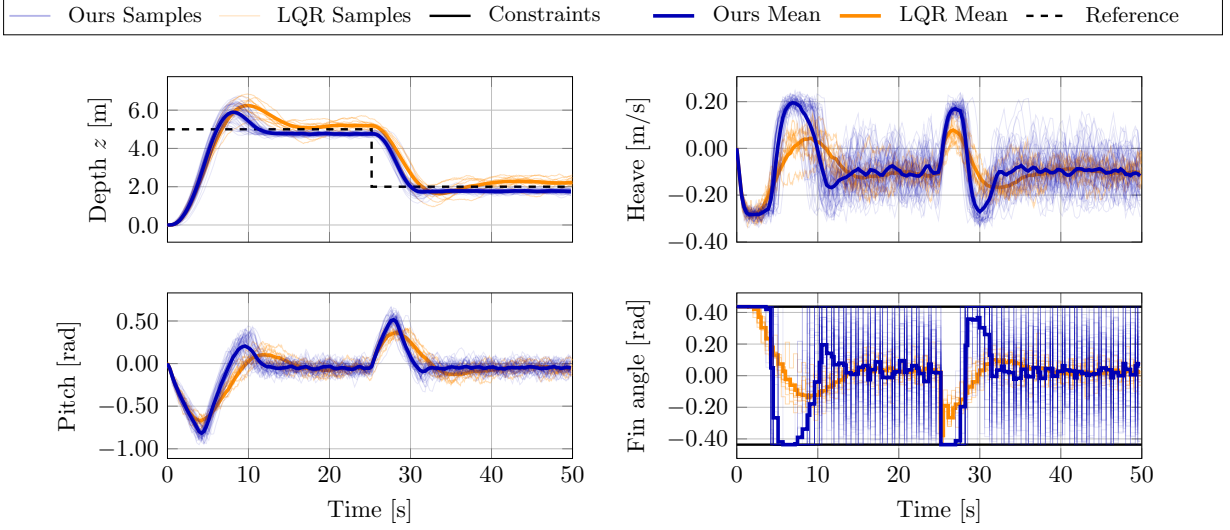


Figure 5: Tracking performance for two depth references $z_{\text{ref}} = (5 \text{ m}, 2 \text{ m})$, switching at $t = (0 \text{ s}, 25 \text{ s})$, is evaluated over $M = 50$ simulation runs of the closed-loop SDE under the learned control law $\hat{\pi}^*$ with $\epsilon = 0.001$ and compared to LQR.

exact knowledge of the system parameters and performs well because it represents an exact linearization at the operating point reached after the transient, due to the translational invariance of depth in the nonlinear dynamics. In contrast, our control law $\hat{\pi}$ is learned entirely from data without access to the system model or its parameters, yet achieves lower costs and reduced variability by exploiting the full nonlinear dynamics.

5. Conclusion

This paper has presented a fully data-driven framework for approximating optimal feedback laws in stochastic optimal control problems. This approach *scales linearly with states*, thereby enabling polynomial runtime complexity of both the identification as well as control, as summarized in Table 1. The Kernel HJB recursion and operator model learning offer a promising avenue for addressing high-dimensional and uncertain optimal control problems. This versatility opens a variety of future research directions, including large-scale regression via data-efficient low-rank estimators and feature spaces for further reduction of the computational complexity of the proposed algorithms.

References

Astrom, K.J., Wittenmark, B., 1994. Adaptive control. Addison-Wesley Longman Publishing Co., Inc.

Bertsekas, D., Shreve, S.E., 1996. Stochastic optimal control: the discrete-time case. volume 5. Athena Scientific.

Bevanda, P., Driessens, B., Iacob, L.C., Sosnowski, S., Tóth, R., Hirche, S., 2025a. Nonparametric control Koopman operators. arXiv preprint arXiv:2405.07312 [arXiv:2405.07312](https://arxiv.org/abs/2405.07312).

Bevanda, P., Hoischen, N., Wittmann, T., Brudigam, J., Hirche, S., Houska, B., 2025b. Kernel-based optimal control: An infinitesimal generator approach, in: Proceedings of the 7th Annual Learning for Dynamics and Control Conference, PMLR. pp. 1038–1052.

Bogachev, V., Krylov, N., Röckner, M., Shaposhnikov, S., 2015. Fokker-Planck-Kolmogorov equations. AMS.

Bruder, D., Fu, X., Gillespie, R.B., Remy, C.D., Vasudevan, R., 2020. Data-driven control of soft robots using Koopman operator theory. *IEEE transactions on robotics* 37, 948–961.

Caldarelli, E., Chatalic, A., Colomé, A., Molinari, C., Ocampo-Martinez, C., Torras, C., Rosasco, L., 2025. Linear quadratic control of nonlinear systems with Koopman operator learning and the nyström method. *Automatica* 177, 112302.

Coulson, J., Lygeros, J., Dörfler, F., 2019. Data-enabled predictive control: In the shallows of the deepc, in: 2019 18th European control conference (ECC), IEEE. pp. 307–312.

Crandall, M.G., Ishii, H., Lions, P.L., 1992. User's guide to viscosity solutions of second order partial differential equations. *Bulletin of the American mathematical society* 27, 1–67.

Diehl, M., Ferreau, H.J., Haverbeke, N., 2009. Efficient Numerical Methods for Nonlinear MPC and Moving Horizon Estimation. Springer Berlin Heidelberg, Berlin, Heidelberg. pp. 391–417.

Doyle, J., Primbs, J.A., Shapiro, B., Nevistic, V., 1996. Nonlinear games: examples and counterexamples, in: 35th Conference on Decision and Control, IEEE. pp. 3915–3920.

Fleming, W., Soner, H., 1993. Controlled Markov Processes and Viscosity Solutions. Springer.

Guo, Y., Houska, B., Villanueva, M.E., 2022. A tutorial on Pontryagin-Koopman operators for infinite horizon optimal control, in: 61st Conference on Decision and Control (CDC), IEEE. pp. 6800–6805.

Henrion, D., Lasserre, J.B., Savorgnan, C., 2008. Nonlinear optimal control synthesis via occupation measures, in: 47th Conference on Decision and Control, IEEE. pp. 4749–4754.

Hewing, L., Kabzan, J., Zeilinger, M.N., 2019. Cautious model predictive control using Gaussian process regression. *IEEE Transactions on Control Systems Technology* 28, 2736–2743.

Hinze, M., Pinna, R., Ulbrich, M., Ulbrich, S., 2009. Optimization with PDE Constraints. Springer.

Houska, B., 2025. Convex operator-theoretic methods in stochastic control. *Automatica* 177, 112274.

Klus, S., Schuster, I., Muandet, K., 2020. Eigendecompositions of transfer operators in reproducing kernel Hilbert spaces. *Journal of Nonlinear Science* 30, 283–315.

Koopman, B.O., 1931. Hamiltonian systems and transformation in Hilbert space. *Proceedings of the National Academy of Sciences* 17, 315–318.

Korda, M., Mezić, I., 2018. Linear predictors for nonlinear dynamical systems: Koopman operator meets model predictive control. *Automatica* 93, 149–160.

Kostic, V., Lounici, K., Novelli, P., Pontil, M., 2023. Sharp spectral rates for Koopman operator learning. *Advances in Neural Information Processing Systems* 36, 32328–32339.

Kostic, V., Novelli, P., Maurer, A., Ciliberto, C., Rosasco, L., Pontil, M., 2022. Learning dynamical systems via Koopman operator regression in reproducing kernel Hilbert spaces. *Advances in Neural Information Processing Systems* 35, 4017–4031.

Krylov, N., 2008. Controlled diffusion processes. Springer.

Li, Q., Dietrich, F., Boltt, E.M., Kevrekidis, I.G., 2017. Extended dynamic mode decomposition with dictionary learning: A data-driven adaptive spectral decomposition of the Koopman operator. *Chaos: An Interdisciplinary Journal of Nonlinear Science* 27.

Muandet, K., Fukumizu, K., Sriperumbudur, B., Schölkopf, B., et al., 2017. Kernel mean embedding of distributions: A review and beyond. *Foundations and Trends® in Machine Learning* 10, 1–141.

Naik, M.S., Singh, S.N., 2007. State-dependent riccati equation-based robust dive plane control of auv with control constraints. *Ocean Engineering* 34, 1711–1723.

Oksendal, B., 2000. Stochastic Differential Equations. Springer.

Schulman, J., Wolski, F., Dhariwal, P., Radford, A., Klimov, O., 2017. Proximal policy optimization algorithms. *arXiv preprint arXiv:1707.06347* .

Song, Y., Romero, A., Müller, M., Koltun, V., Scaramuzza, D., 2023. Reaching the limit in autonomous racing: Optimal control versus reinforcement learning. *Science Robotics* 8, eadg1462.

Steinwart, I., Christmann, A., 2008. Support Vector Machines. Information Science and Statistics. first ed., Springer, New York, NY.

Strässer, R., Berberich, J., Allgöwer, F., 2023. Robust data-driven control for nonlinear systems using the Koopman operator. *IFAC-PapersOnLine* 56, 2257–2262.

Vaidya, U., Tellez-Castro, D., 2023. Data-driven stochastic optimal control with safety constraints using linear transfer operators. *IEEE Transactions on Automatic Control* 69, 2100–2115.

Vinter, R., 1993. Convex duality and nonlinear optimal control. *SIAM journal on control and optimization* 31, 518–538.

Williams, M.O., Kevrekidis, I.G., Rowley, C.W., 2015. A data–driven approximation of the Koopman operator: Extending dynamic mode decomposition. *Journal of Nonlinear Science* 25, 1307–1346.